Published OnlineFirst December 1, 2020; DOI: 10.1158/1078-0432.CCR-20-3392

Preclinical Characterization of HPN536, a Trispecific, T-Cell–Activating Protein Construct for the Treatment of Mesothelin-Expressing Solid Tumors

Mary Ellen Molloy[1], Richard J. Austin[1], Bryan D. Lemon[1], Wade H. Aaron[1], Vaishnavi Ganti[1], Adrie Jones[1], Susan D. Jones[1], Kathryn L. Strobel[1], Purbasa Patnaik[1], Kenneth Sexton[1], Laurie Tatalick[1], Timothy Z. Yu[1], Patrick A. Baeuerle[1,2,3], Che-Leung Law[1], and Holger Wesche[1]

ABSTRACT

Purpose: Mesothelin (MSLN) is a glycophosphatidylinositol-linked tumor antigen overexpressed in a variety of malignancies, including ovarian, pancreatic, lung, and triple-negative breast cancer. Early signs of clinical efficacy with MSLN-targeting agents have validated MSLN as a promising target for therapeutic intervention, but therapies with improved efficacy are still needed to address the significant unmet medical need posed by MSLN-expressing cancers.

Experimental Design: We designed HPN536, a 53-kDa, trispecific, T-cell–activating protein-based construct, which binds to MSLN-expressing tumor cells, CD3ε on T cells, and to serum albumin. Experiments were conducted to assess the potency, activity, and half-life of HPN536 in *in vitro* assays, rodent models, and in nonhuman primates (NHP).

Results: HPN536 binds to MSLN-expressing tumor cells and to CD3ε on T cells, leading to T-cell activation and potent redirected target cell lysis. A third domain of HPN536 binds to serum albumin for extension of plasma half-life. In cynomolgus monkeys, HPN536 at doses ranging from 0.1 to 10 mg/kg demonstrated MSLN-dependent pharmacologic activity, was well tolerated, and showed pharmacokinetics in support of weekly dosing in humans.

Conclusions: HPN536 is potent, is well tolerated, and exhibits extended half-life in NHPs. It is currently in phase I clinical testing in patients with MSLN-expressing malignancies (NCT03872206).

Introduction

Redirection of cytotoxic T cells with bispecific antibody constructs for cancer therapy has been validated in the clinic (1–6). Blinatumomab is the first and thus far the only bispecific T-cell engager (BiTE) approved by the FDA (7). T-cell–engaging biologics function by forming an immunologic cytolytic synapse between cancer target cells and T cells, which leads to target cell lysis independent of T-cell receptor (TCR) specificity, peptide antigen presentation by HLA, and T-cell costimulation. Despite the clinical success of blinatumomab for treating relapsed and refractory acute lymphoblastic leukemia, other molecules, including BiTE antibodies, showed only limited activity in the treatment of solid tumors (8, 9). Their short plasma half-life required continuous intravenous infusion limiting their utility for most solid tumor indications. Novel designs for T-cell–engaging antibodies aim at overcoming limitations of the first generation and are already being tested in clinical trials (10).

The Trispecific T-cell–Activating Construct (TriTAC) design has been specifically developed to treat solid tumors (11). TriTACs consist of a single polypeptide chain aligning three humanized, antibody-derived binding domains: a single-domain antibody (sdAb) specific for a tumor antigen, a sdAb specific for serum albumin for half-life extension, and a single-chain fragment variable (scFv) specific for the CD3ε subunit of the TCR complex (11). Their molecular size of 53 kDa is about one-third of that of an IgG. Binding of TriTACs to tumor antigen and CD3ε is monovalent, which minimizes off-target CD3ε clustering that can potentially lead to nonspecific T-cell activation. The absence of an Fc-gamma domain for half-life extension is functionally compensated by an albumin-binding domain. HPN424 (11) and HPN536, the first two TriTACs are in phase I clinical testing in hormone refractory prostate cancer and mesothelin (MSLN)-overexpressing solid tumors, respectively.

Human MSLN is produced as a 71-kDa precursor of 628 amino acids, which is expressed as a glycophosphatidylinositol-linked cell surface glycoprotein. Its 31-kDa N-terminal domain is released as a soluble protein, termed as the megakaryocyte potentiating factor (MPF), while the 40-kDa C-terminal domain remains attached to the plasma membrane as mature MSLN (12–14). MSLN expression on normal tissue is confined to the single-cell mesothelial layer covering the surface of tissues and organs of the pleural, pericardial, and peritoneal cavities (13, 15). MUC16/CA125 is a binding partner for MSLN, implicating a role for MSLN in cell adhesion (16, 17). However, the precise physiologic functions of MSLN have not been defined, and MSLN-knockout mice exhibit no detectable phenotype or developmental abnormality (18).

MSLN is overexpressed in many malignancies, including ovarian cancer (13, 15, 19), pancreatic cancer (20, 21), non–small cell lung cancer (22–26), triple-negative breast cancer (26, 27), and mesothelioma (28, 29). In triple-negative breast cancer (25) and in lung and pancreatic adenocarcinomas (22, 23, 30), overexpression of MSLN correlates with poor prognosis. Differential expression of MSLN in cancer versus normal tissue has made it an attractive target for MSLN-directed imaging agents and therapeutics (10, 31–33). A challenge in developing MSLN-directed therapeutics is the expression of MSLN on normal mesothelial cells, potentially leading to dose-limiting toxicities.

[1]Harpoon Therapeutics, South San Francisco, California. [2]MPM Capital, Cambridge, Massachusetts. [3]Institute for Immunology, Ludwig-Maximilians University Munich, Planegg- Martinsried, Munich, Germany.

Note: Supplementary data for this article are available at Clinical Cancer Research Online (http://clincancerres.aacrjournals.org/).

Corresponding Author: Mary Ellen Molloy, Harpoon Therapeutics, 131 Oyster Point Boulevard, 300, South San Francisco, CA 94080. Phone: 773-318-0796; E-mail: mmolloy@harpoontx.com

Clin Cancer Res 2020;XX:XX–XX

doi: 10.1158/1078-0432.CCR-20-3392

Published OnlineFirst December 1, 2020; DOI: 10.1158/1078-0432.CCR-20-3392

Translational Relevance

Patients with mesothelin (MSLN)-overexpressing tumors, including ovarian, pancreatic, lung, and triple-negative breast cancer, have a high unmet clinical need. A number of MSLN-targeted therapeutics have been developed that show limited efficacy and safety in clinical trials. HPN536 is a novel, MSLN-targeted, trispecific, T-cell–activating protein construct that can potently redirect T cells to lyse tumor cells and was remarkably well tolerated in nonhuman primates at single doses up to 10 mg/kg, which is far above the expected therapeutic dose level. Our findings suggest that HPN536 has the potential for high clinical activity and a wide therapeutic window. Its long serum half-life supports once-weekly dosing in humans. Currently, HPN536 is the only MSLN-targeting, T-cell–engaging biologic in clinical testing.

HPN536 specifically redirects T cells for potent redirected lysis of MSLN-expressing cancer cells with concomitant T-cell activation. In three different mouse xenograft models, HPN536 induced durable antitumor activity at very low doses. In cynomolgus monkeys, HPN536 was well tolerated, showed a long serum half-life, and elicited signs of target engagement on mesothelial structures.

Materials and Methods

Protein production

Sequences of TriTACs, sdAbs, and extracellular domains of target proteins fused to an Fc domain or a hexahistidine tag were cloned into mammalian expression vector, pcDNA 3.4 (Invitrogen), preceded by a leader sequence. Expi293 Cells (Life Technologies) were maintained in suspension in Optimum Growth Flasks (Thomson) between 0.2 and 8×10^6 cells/mL in Expi293 media. Purified plasmid DNA was transfected into Expi293 cells in accordance with Expi293 Expression System Kit (Life Technologies) protocols and cultured for 4–6 days after transfection. Alternatively, HPN536 was produced in CHO-DG44 DHFR–deficient cells (34). The amount of expressed proteins in conditioned media was quantitated using an Octet RED96 instrument with Protein A Tips (ForteBio/Pall) using appropriate purified control proteins for a standard curve. Conditioned media from either host cell were filtered and purified by protein A affinity and desalted or subjected to preparative size exclusion chromatography (SEC) using an AKTA Pure Chromatography System (GE Healthcare). Protein A purified TriTAC proteins were further purified by ion exchange and formulated in a buffered solution containing excipients. Final purity was assessed by SDS-PAGE by resolving 2.5 μg/lane on TRIS-Glycine gels and visualized with Simply Blue Stain (Life Technologies). Native purity was also assessed by analytic SEC using a Yarra SEC150 3 μm 4.6 × 150 mm Column (Phenomenex) resolved in an aqueous/organic mobile phase buffered at neutral pH on a 1290 LC system and peaks were integrated with OpenLab ChemStation Software (Agilent Technologies).

In vitro affinity measurements

Affinities of HPN536 analyte for albumin, CD3ε, and MSLN ligands were measured by biolayer interferometry using an Octet RED96 instrument with Streptavidin Tips (ForteBio/Pall). Experiments were performed at 27°C in PBS plus casein in the absence or presence of 15 mg/mL has, as described in Results section and figure legends. Binding sensograms generated from empirically determined ligand loads, appropriate serial dilutions of known analyte concentrations, and association and dissociation times were then fit globally to a one-to-one binding model using Octet DataAnalysis 9.0 software.

In vitro T-cell–dependent cell cytotoxicity and T-cell activation assays

T cells from healthy donors were purified from leukopaks (leukapheresis samples, StemCell Technologies) using EasySep Human T Cell Isolation Kits (StemCell Technologies, 17951) following the manufacturer's instructions. All cancer cell lines were obtained from the ATCC, with the exception of OVCAR8 cells, which were obtained from the NCI (Bethesda, MD). Cell lines were passaged a maximum of 36 times after being received from the ATCC. Cell line authentication and *Mycoplasma* testing were not performed. T-cell–dependent cell cytotoxicity (TDCC) assays were performed as described previously (35). Briefly, luciferase-expressing target cells and purified human T cells were seeded per well of a 384-well plate at a 10:1 T cell-to-target cell ratio. Target cell killing was assessed following incubation for 48 hours at 37ºC and 5% CO_2. Target cell viability was assessed by incubation with the SteadyGlo Reagent (Promega). Luminescence was measured using a PerkinElmer EnVision Detection System. Activated T cells were identified by CD69 and CD25 surface expression (BD Biosciences). Samples were analyzed on a FACSCelesta Flow Cytometer (BD Biosciences). Flow cytometry data were processed using FlowJo v10 Software (FlowJo, LLC).

Binding of HPN536 on MSLN-expressing OVCAR and T cells

Cultured cells were incubated with 1 μg/mL HPN536 or anti-GFP TriTAC (control) for 1 hour. Binding was detected using Alexa647-anti-TriTAC antibody using a FACSCelesta Flow Cytometer (BD Biosciences). The QIFIKIT (Dako) was used according to the manufacturer's instructions to estimate the number of MSLN molecules expressed per cell.

Cytokines in the presence of T cells

To measure the cytokines, AlphaLISA Kits were used (PerkinElmer) per the manufacturer's instructions, except that the assays were performed in 384-well plates instead 96-well plates. Plates containing conditioned media from TDCC assays were used for analysis. Plates were read on a PerkinElmer EnVision Plate Reader equipped with an AlphaLISA module.

In vivo mouse efficacy studies

All mouse studies were performed in accordance with the policies of the Institutional Animal Care and Use Committee (IACUC) at Harpoon Therapeutics and Charles River Laboratories. For TOV21G and HPAFII experiments, NCG (NOD-*Prkdc*^{em26Cd52}*Il2rg*^{em26Cd22}/NjuCrl) mice received subcutaneous coimplants of human cancer cells (5×10^6) and human T cells (5×10^6) in 50% Matrigel (BD Biosciences) on day 0. Human T cells were expanded before implantation using Human T Cell Activation/Expansion Kit (Miltenyi Biotec) according to the manufacturer's instructions. Mice were dosed on days 1–15 (HPAFII, **Fig. 4A** and TOV21G, **Fig. 4C**) or days 7–16 (HPAFII, **Fig. 4B**) via intraperitoneal injection. For NCI-H292 experiments, NCG mice received subcutaneous coimplants of human cancer cells (1×10^7) and human peripheral blood mononuclear cells (PBMC; 1×10^7). Mice were administered HPN536 daily for 10 days starting on day 6 via intravenous injection. Tumor size was measured twice weekly and calculated using the following formula: tumor volume (mm^3) = $(w^2 \times l)/2$. Percent tumor growth inhibition (%TGI) was defined as the difference between the mean tumor volume (MTV) of the control

Published OnlineFirst December 1, 2020; DOI: 10.1158/1078-0432.CCR-20-3392

group and the MTV of the treated group, expressed as a percentage of the MTV of the control group.

Exploratory cynomolgus monkey dose range–finding study

The pharmacology, pharmacokinetics, and toxicity of HPN536 were evaluated after a single intravenous bolus dose of 0.1, 1.0, or 10 mg/kg HPN536 in one male and one female cynomolgus monkey per group followed by either a 1- or 3-week postdose recovery period. The study followed the protocol and standard operating procedures of the testing facility (Charles River Laboratories) and was approved by their IACUC. Pharmacologic activity was evaluated by clinical observations, cytokine assessments, flow cytometry, and evidence of target engagement by histology. Two research electrochemiluminescence assays, a functional assay and an anti-idiotype assay, were used for measuring HPN536 levels in serum. For the functional assay, HPN536 was captured with biotinylated CD3ε and was detected with a sulfo-tagged MSLN. For the anti-idiotype assay, HPN536 was captured with an anti-idiotype antibody recognizing the anti-albumin domain and was detected with a sulfo-tagged CD3ε. Toxicokinetic parameters were estimated using Phoenix WinNonlin pharmacokinetic software. A noncompartmental approach, consistent with the intravenous bolus route of administration, was used for parameter estimation. Toxicity endpoints included daily morbidity and mortality, daily clinical observations, weekly body weights, daily food consumption, clinical pathology (hematology, clinical chemistry, and coagulation), and anatomic pathology (gross necropsy, organ weights, and histopathology).

Results

Production, structure, and biochemical characteristics of HPN536

Recombinant HPN536 has a molecular weight of approximately 53 kDa. A humanized llama sdAb specific for human MSLN is placed at its N-terminus (**Fig. 1A**). A humanized llama sdAb specific for human serum albumin (HSA) is placed in the middle of the molecule. The C-terminal end contains a humanized scFv specific for the human CD3ε subunit of the TCR complex. GGGGSGGGS linkers connect the three binding domains.

HPN536 is produced by eukaryotic cell culture and secreted as a single, nonglycosylated polypeptide. Stability studies subjecting HPN536 to various stress conditions, including multiple freeze thaw cycles and storage at 4°C and 40°C for 2 weeks, suggest the protein is stable and stress resistant (Supplementary Fig. S1). The high stability of HPN536 ensures limited aggregation, which would otherwise lead to

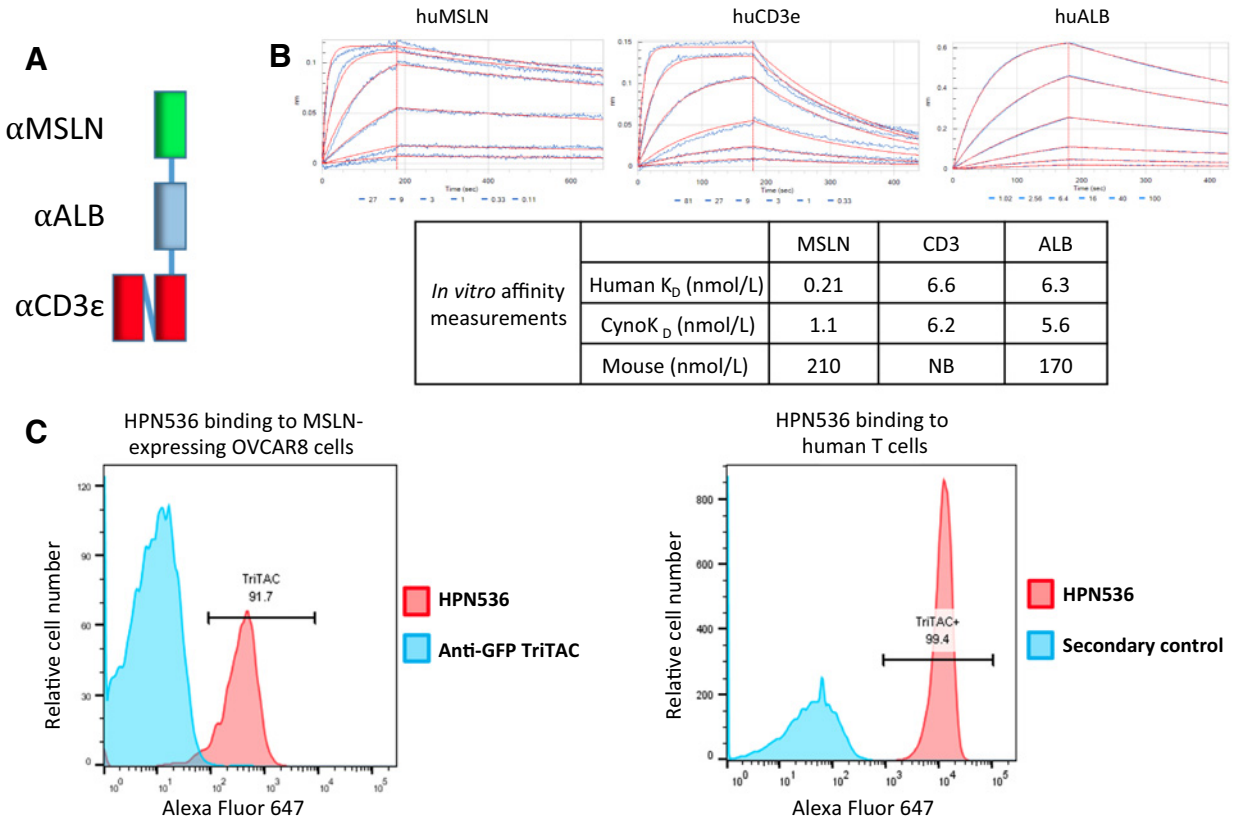

		MSLN	CD3	ALB
In vitro affinity measurements	Human K_D (nmol/L)	0.21	6.6	6.3
	CynoK_D (nmol/L)	1.1	6.2	5.6
	Mouse (nmol/L)	210	NB	170

Figure 1.

Binding of HPN536 to MSLN, albumin (ALB), and CD3ε (CD3). **A,** Schematic illustration of HPN536 as a trispecific molecule consisting of an anti-MSLN sdAb that targets cells expressing MSLN (αMSLN), an anti-albumin sdAb that extends half-life (αALB), and an anti-CD3ε scFv that engages T cells (αCD3ε). **B,** HPN536 affinity for three targets as assessed by biolayer interferometry. Representative curves are shown for human MSLN (huMSLN), CD3ε (huCD3ε), and HSA (huALB). The red curves in each panel represent a global fit of the data to a one-to-one binding model with decreasing concentrations indicated from top to bottom. The table summarizes HPN536 affinity to human, cynomolgus monkey, and mouse targets for replicate experiments. NB, no binding. **C,** FACS binding of HPN536 to MSLN-expressing OVCAR8 and human T cells.

Published OnlineFirst December 1, 2020; DOI: 10.1158/1078-0432.CCR-20-3392

CD3 clustering and nonspecific T-cell activation in the absence of target cells, and potential off-target side effects.

Biolayer interferometry analysis demonstrated that HPN536 binds with high affinity to recombinant or purified human and cynomolgus monkey MSLN, CD3ε, and albumin in the range of 0.21–6.7 nmol/L (**Fig. 1B**). The K_D values for binding to human and cynomolgus monkey orthologs were found to be within 6-fold of each other for all three target antigens. HPN536 bound to mouse MSLN and albumin with equilibrium binding constants of 210 and 170 nmol/L, respectively, but did not detectably bind mouse CD3ε (**Fig. 1B**). As demonstrated by flow cytometry analysis, HPN536 exhibited surface binding to human MSLN-expressing OVCAR cells and purified human T cells, confirming that HPN536 recognized native MSLN and CD3ε expressed on cells (**Fig. 1C**).

Redirected tumor cell lysis by HPN536 in cocultures

The *in vitro* potency of HPN536 was evaluated in a TDCC assay. Primary resting human T cells were combined with target cells at a ratio of 10:1, incubated for 48 hours, and the viability of target cells was determined. In cocultures of MSLN-expressing OVCAR3 ovarian cancer cells and resting T cells from five different donors, HPN536 efficiently directed T cells to lyse OVCAR3 target cells with EC_{50} values ranging from 1.3 to 2.5 pmol/L (**Fig. 2A**; Supplementary Table S1). No lysis of OVACR3 cells was observed with a control TriTAC specific for GFP, showing that sole binding to CD3ε on T cells was not sufficient to mediate cytotoxicity. HPN536 also redirected T cells for lysis of other ovarian cancer cell lines expressing MSLN, including Caov3, Coav4, and OVCAR8, but it was inactive against MSLN-negative cell lines MDAPCa2b and NCI-510A, demonstrating strict specificity for MSLN (**Fig. 2B**; Supplementary Table S1). Because HPN536 contains an anti-albumin binder for half-life extension, TDCC assay was conducted in the presence of physiologic levels of serum albumin. Serum albumin did not inhibit the ability of HPN536 to redirect human T cells to kill MSLN-expressing target cells and had a minimal impact on potency (Supplementary Fig. S2).

Lysis by HPN536-engaged T cells was further explored with MSLN-expressing tumor cell lines of different histologic origins, including three pancreatic (Hs766T, Capan-2, and HPAFII; **Fig. 2C**; **Table 1**), three non–small cell lung cancer (NCI-H596, NCI-H292, and NCI-H1563; **Fig. 2D**; **Table 1**), and two mesothelioma cell lines (NCI-H2052 and NCI-H2452; **Table 1**). EC_{50} values of HPN536 for redirected lysis ranged from 2.3 to 15 pmol/L across the various cell lines. HEK 293 cells, genetically engineered to express either human or cynomolgus monkey MSLN, were killed with EC_{50} values of 0.9 and 0.7 pmol/L, respectively. PBMCs from cynomolgus monkeys were also able to kill MSLN-expressing tumor cells in the presence of HPN536 (Supplementary Fig. S3). These data support the use of cynomolgus monkey as a relevant species for toxicology studies with HPN536. **Table 1** summarizes the EC_{50} values across all cell lines of different histopathologic origins, as well as an estimate of the number of MSLN molecules expressed per cell as determined by flow cytometry.

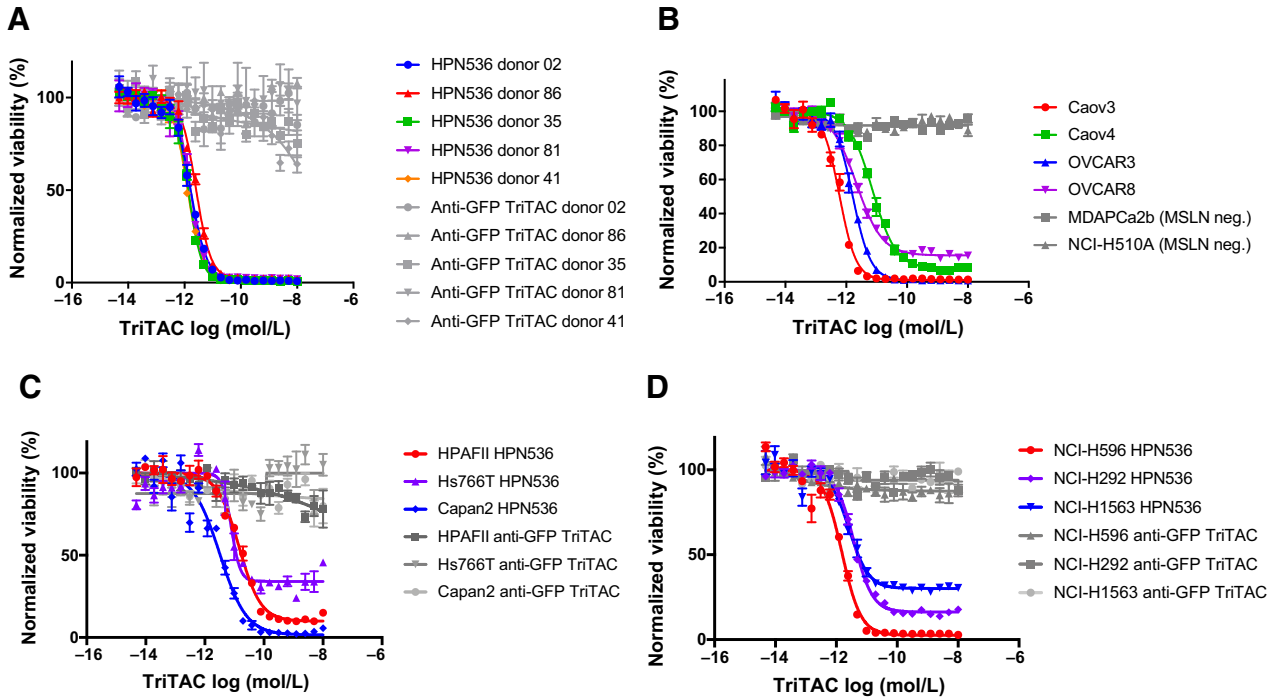

Figure 2.

HPN536 directs T-cell killing in the presence of MSLN-expressing cells. **A,** Luciferase-labeled OVCAR3 cells were incubated with resting human T cells from five different donors at a 1:10 target-to–T cell ratio. Titrations of HPN536 or a negative control, anti-GFP TriTAC protein, were added to the target cell/T-cell cocultures. Forty-eight hours later, viability of the OVCAR3 cells was assessed by measuring luciferase activity. **B,** Luciferase-labeled, MSLN-expressing Caov3, Caov4, OVCAR3, and OVCAR8, and MSLN-negative MDAPCa2b and NCI-510a cells were incubated with resting human T cells at a 1:10 target-to–T-cell ratio. Titrations of HPN536 were added to the target cell/T-cell cocultures. Forty-eight hours later, viability was assessed by measuring luciferase activity. Pancreatic cell lines HPAFII, Hs766T, CaPan2 (**C**) and NSCLC cell lines, NCI-H596, NCI-H292, and NCI-H1563 (**D**) were incubated with resting human T cells at a 1:10 target-to–T-cell ratio. Titrations of HPN536 or a negative control, an anti-GFP TriTAC protein, were added to the target cell/T-cell cocultures. Forty-eight hours later, viability was assessed by measuring luciferase activity.

Published OnlineFirst December 1, 2020; DOI: 10.1158/1078-0432.CCR-20-3392

Table 1. Summary of EC_{50} values from TDCC assays and MSLN sites per cell in different cell lines.

Tumor origin	Cell line	EC_{50} (pmol/L)	MSLN sites per cell
Ovarian	Caov3	0.6	51,262
	Caov4	7.3	101,266
	OVCAR3	1.6	40,589
	OVCAR8	2.2	40,216
	SKOV3	3.6	10,617
	TOV21G	3.2	nd
Pancreatic	Hs766T	7.8	5,892
	CaPan2	3.2	27,413
	HPaFII	15	17,844
NSCLC	NCI-H596	1.5	103,769
	NCI-H292	3.8	5,977
	NCI-H1563	2.6	17,221
Mesothelioma	NCI-H2052	8.0	nd
	NCI-H2452	2.3	nd
Engineered (nontumor)	293 human MSLN	0.9	128,091
	293 cyno MSLN	0.7	140,683

Abbreviations: Cyno, cynomolgus monkey; NSCLC, non–small cell lung cancer.
Note: Luciferase-labeled target cells were incubated with resting human T cells at a 1:10 target-to–T-cell ratio. Titrations of HPN536 or a negative control, a GFP-targeting TriTAC protein, were added to the target cell/T-cell cocultures. Forty-eight hours later, viability of target cells was assessed by measuring luciferase activity. EC_{50} values are expressed in pmol/L concentrations. The QIFIKIT (Dako) was used according to the manufacturer's instructions to estimate the number of MSLN molecules expressed per cell. nd, not determined.

T-cell activation by HPN536

T-cell activation by HPN536 was first assessed by induction of CD69 and CD25 surface expression on T cells. T cells from four normal donors were cocultured with the MSLN-positive cancer cell line, OVCAR8, at various concentrations of HPN536. Within 48 hours, HPN536 mediated a dose-dependent increase in the percentage of CD69- and CD25-positive T cells in coculture with MSLN-positive OVCAR8 cells (**Fig. 3A** and **B**). A GFP-specific TriTAC control had no effect on new CD69 or CD25 expression on T cells. Depending on the T-cell donor, between 5% and 20% of the T cells in culture upregulated CD69 and CD25 surface expression. Similar effects on T-cell activation were observed in coculture with MSLN-positive tumor cell line, Caov3 (Supplementary Fig. S4). The EC_{50} values of HPN536 for upregulation of CD69 and CD25 in the presence of MSLN-positive cancer cells ranged from 0.14 to 9.0 pmol/L (Supplementary Table S2).

T-cell activation was also assessed by the release of inflammatory cytokines by T cells that were cocultured with MSLN-expressing OVCAR8 cancer cells. As shown in **Fig. 3C** and **D**, HPN536 mediated a dose-dependent secretion of TNFα and IFNγ into coculture media. A GFP-specific control TriTAC did not cause cytokine release by T cells. Comparable results were observed with Coav3, Caov4, and OVCAR3 as target cells and with multiple T-cell donors (Supplementary Tables S3 and S4). Of note, induction of CD69 and CD25 and release of cytokines by T cells were not observed in coculture with MSLN-negative tumor cell line, MDAPCa2b (Supplementary Fig. S5).

Antitumor activity of HPN536 in mouse xenograft models

The antitumor activity of HPN536 was assessed in three xenograft mouse models established from cancer types that express MSLN: HPAFII (pancreatic cancer), TOV21G (ovarian cancer), and NCI-H292 (non–small cell lung cancer). A daily dosing regimen was selected on the basis of the reported half-life for mouse serum albumin of approximately 1 day (36, 37). Moreover, HPN536 bound mouse serum albumin with a lower affinity than HSA (K_D values of 170 vs. 6.3 nmol/L, respectively). Consistent with this, the serum half-life of HPN536 in mice was determined to be 24 hours (Supplementary Fig. S6; Supplementary Table S5). In a first study, HPAFII tumor cells were subcutaneously coimplanted with T cells from normal human donors at an effector-to-target cell ratio (E:T) of 1:1 (**Fig. 4A**). Daily doses of HPN536, 100, 20, or 4 μg/kg, were administered over 15 days by intraperitoneal injection starting 1 day after implantation. Doses of 20 and 100 μg/kg HPN536 caused HPAFII tumor eradication, while 4 μg/kg only slightly delayed tumor outgrowth (**Fig. 4A**) compared with a GFP-specific control TriTAC at 100 μg/kg. In a second experiment, HPAFII cancer cells and T cells from a healthy donor at an E:T ratio of 1:1 were coimplanted under the skin, and tumors were allowed to establish for 7 days until they reached an average volume of 170 mm^3 before a 10-day treatment with HPN536 was initiated. On day 24 after tumor implantation, both 500 and 100 μg/kg doses of HPN536 led to eradication of the established HPAFII tumors in mice (**Fig. 4B**).

For the TOV21G tumor model, mice were treated with 500, 100, and 20 μg/kg HPN536 1 day following tumor coimplantation with human T cells. On day 35 postimplantation, 500, 100, and 20 μg/kg HPN536 treatment groups showed TGI of 65.1%, 68.6%, and 52.3%, respectively, and delayed tumor outgrowth with high statistical significance (**Fig. 4C**). For the NCI-H292 model, tumor cells were coimplanted with human PBMCs and tumors were allowed to grow for 6 days, at which point the tumor volume reached about 27 mm^3, before treatment was initiated. On day 6, HPN536 was administered at daily doses of 500, 100, and 20 μg/kg for 10 days. A highly significant tumor inhibition was seen in both the 100 and 500 μg/kg HPN536-treated groups compared with the vehicle-treated group (70.9% and 77.1% TGI, respectively; **Fig. 4D**). These results demonstrate activity of HPN536 in controlling growth of MSLN-expressing tumors derived from different histologic origins.

Pharmacokinetics of HPN536 in cynomolgus monkeys

On the basis of the species cross-reactivity of HPN536 to cynomolgus monkey MSLN, CD3, and albumin (see **Fig. 1**), the pharmacokinetics of a single dose of 0.1, 1, or 10 mg/kg was evaluated in cynomolgus monkeys (two males and two females per dose group). An anti-idiotype assay (anti-anti-albumin used for capture and anti-anti-CD3 for detection) and a functional assay (recombinant CD3 and MSLN proteins used for capture and detection, respectively) were used for detection of HPN536. The serum concentration–time profile for HPN536 exhibited a biphasic decline for the dose range 0.1–10 mg/kg over the time course of the study (**Fig. 5A**). Noncompartmental analysis of HPN536 exhibited a dose proportional increase in maximum serum concentration (C_{max}) and area under the concentration–time curve (AUC_{0-inf}). In addition, the volume of distribution at steady state was independent of dose. The clearance rate was in the range of 0.57–1.39 mL/hour/kg and the mean terminal half-life was between 49.0 and 113 hours, supporting the hypothesis that the HSA binding domain engaged its target HSA to extend the serum half-life of HPN536 (Supplementary Table S6). The time–concentration profiles determined with the two different assays overlaid (**Fig. 5A**), suggesting that HPN536 had retained its structural and functional integrity in cynomolgus monkeys over the course of the 3-week study. To examine *in vivo* stability and biological activity, HPN536-containing serum samples collected after 168 hours of post-HPN536 administration were tested for redirected tumor cell lysis in the TDCC assay. As shown

Published OnlineFirst December 1, 2020; DOI: 10.1158/1078-0432.CCR-20-3392

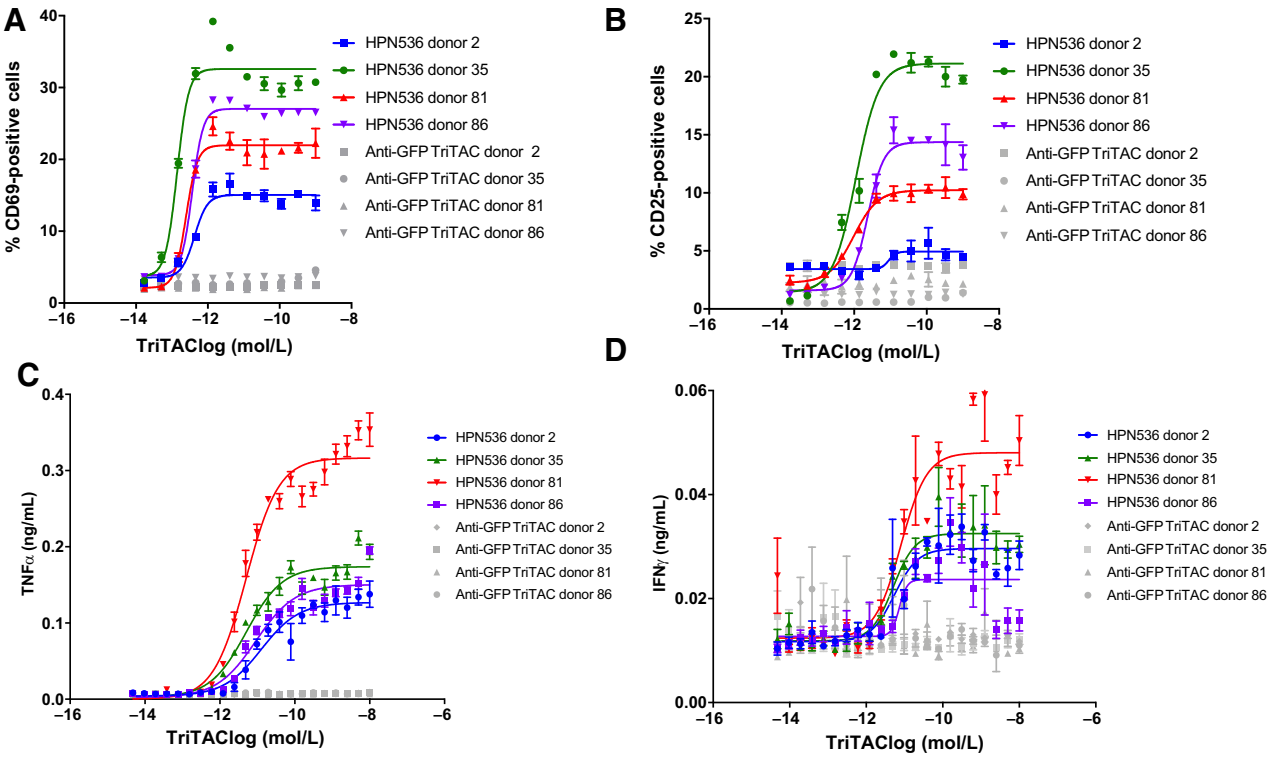

Figure 3.

HPN536 directs T-cell activation in the presence of MSLN-expressing cells. OVCAR8 ovarian cancer cells were incubated with resting human T cells from four different donors. Titrations of HPN536 or a negative control, anti-GFP TriTAC protein, were added to the target cell/T-cell cocultures. Forty-eight hours later, expression of CD69 (**A**) and CD25 (**B**) was measured by flow cytometry. TNFα (**C**) or IFNγ (**D**) levels were also measured in the conditioned media collected from the cocultures.

in **Fig. 5B**, HPN536 contained in the 168-hour serum samples from monkeys was as potent in the TDCC assay as the HPN536 reference stored at −80°C.

Pharmacodynamics and toxicology of HPN536 in cynomolgus monkeys

Single doses of HPN536 were well tolerated in nonhuman primates (NHP) up to 10 mg/kg and no dose-limiting toxicities were observed. HPN536 administration resulted in transient, non-adverse changes in clinical pathology parameters (**Fig. 5C**–E; Supplementary Table S7) and cytokines. Consistent with T-cell activation by HPN536, transient mild to moderate decreases in circulating lymphocytes were observed between days 1 and 2 after drug administration that trended back to control or baseline values by days 3 or 8 (Supplementary Table S7). They included Th lymphocytes, cytotoxic T lymphocytes, natural killer cells, and B lymphocytes as observed by flow cytometry. **Figure 5C** exemplifies a transient reduction in T lymphocytes that recovered by 168 hours after drug administration. A small fraction of T cells showed upregulation of T-cell activation marker, CD69, in response to HPN536 that was not seen in vehicle-treated animals (**Fig. 5D**). T-cell activation in response to HPN536 was also evident from a dose-dependent increase in the inflammatory cytokine, IL6, in serum (**Fig. 5E**). At 10 mg/kg, IL6 levels peaked between 4 and 8 hours after HPN536 administration and had declined by 24 hours after dose. Increases in serum levels of IFNγ and IL2 were also observed between 4 and 8 hours after dose in a subset of animals treated at 10 mg/kg (Supplementary Fig. S7). No consistent changes in serum levels were observed for other cytokines, including IL4, IL5, IL10, and TNFα (Supplementary Fig. S7).

Single doses of HPN536 did not elicit gross pathologic changes or dose-limiting toxicities. The main histopathologic finding was a moderate, dose-dependent mesothelial hypertrophy accompanied by a mixed immune cell infiltration and extracellular matrix deposition. This effect was most pronounced in animals treated at the highest dose level of 10 mg/kg HPN536. **Figure 6** compares a microscopic section through the pulmonary mesothelial layer of an animal receiving a 10 mg/kg dose (middle) with a section from a vehicle-treated animal (left). These HPN536-related mesothelial changes were observed in fewer tissues and at a lower incidence and/or severity 3 weeks after dosing when compared with findings at 1-week after dosing, possibly reflecting reversibility of the histopathologic effect (**Fig. 6**, middle and right).

Discussion

Multiple MSLN-targeted therapies for the treatment of MSLN-expressing malignancies have entered clinical development in recent years (38, 39). These include the antibody amatuximab (40), MSLN-based vaccines (41, 42), chimeric antigen receptor (CAR)-T cells (32), immunotoxins (33), and antibody–drug conjugates (43). Some clinical benefit has been reported for the immunotoxin, SS1P (33, 44, 45), and the antibody–drug conjugate, DMOT4039A (46). Likewise, MSLN-specific CAR-T cells have shown some benefit after intraperitoneal administration to patients with mesothelioma in combination with an anti-PD-1 antibody (32, 47, 48). Challenges of current MSLN-targeted therapies are low response rates and narrow therapeutic windows. To

Published OnlineFirst December 1, 2020; DOI: 10.1158/1078-0432.CCR-20-3392

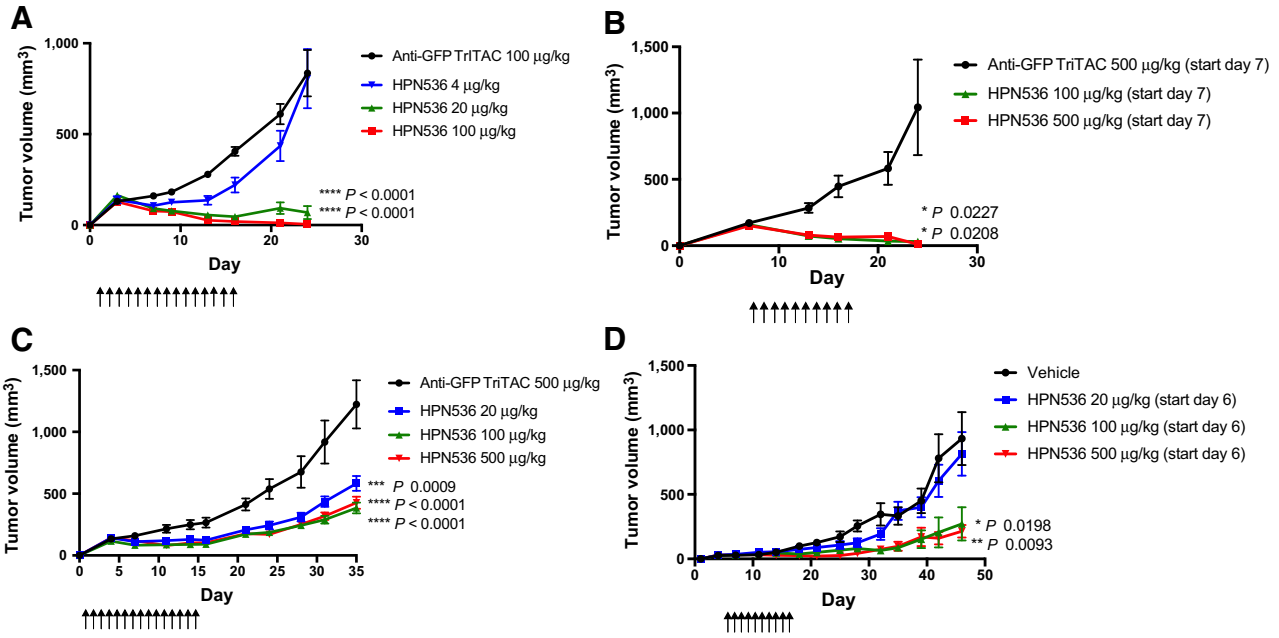

Figure 4.

HPN536 effectively inhibits the growth of multiple cancer types. **A,** HPAFII and T cells expanded from a healthy donor were coimplanted on day 0 at an E:T of 1:1 and treated with HPN536 (4, 20, or 100 μg/kg) or anti-GFP TriTAC (100 μg/kg) on days 1–15 ($n = 10$). **B,** HPAFII and T cells expanded from a healthy donor were coimplanted on day 0 at an E:T of 1:1 and allowed to grow for 7 days until they reached a volume of 170 mm^3. Mice were treated with HPN536 (100 or 500 μg/kg) and anti-GFP TriTAC (500 μg/kg) for 10 days ($n = 5$). **C,** TOV21G cells were coimplanted with T cells expanded from a healthy donor at an E:T of 1:1 on day 0 and treated with HPN536 (20, 100, or 500 μg/kg) or anti-GFP TriTAC (500 μg/kg) on days 1–15 ($n = 10$). **D,** NCI-H292 cells were coimplanted with PBMCs from a healthy donor at an E:T of 1:1 and allowed to grow for 6 days, at which point the tumor volume reached 27 mm^3. Treatment with HPN536 (20, 100, or 500 μg/kg) or vehicle was initiated on day 6 and continued daily to day 16 ($n = 8$). Upward pointing arrows indicate dosing. One-way ANOVA followed by Tukey *post hoc* test using Prism version 7 software was used for statistical analyses.

overcome these, we have generated HPN536, which currently is the only T-cell–engaging antibody construct in clinical testing in patients with MSLN-expressing cancers.

While many T-cell engager formats in development rely on an Fc-gamma domain for half-life extension, HPN536 utilizes an sdAb binding to HSA. Here, we show that the sdAb can confer a prolonged serum half-life of the 53-kDa TriTAC, for up to 113 hours in NHPs. In contrast, the 55-kDa BiTE antibody, blinatumomab, had a serum half-life of only 2 hours in patients and, therefore, required continuous intravenous infusions (7, 49). A weekly or perhaps less frequent dosing schedule may be sufficient to maintain appropriate plasma drug concentration of HPN536 for antitumor activity in the clinic, which would overcome a limitation of the canonical BiTE format. Of note, the *in vitro* biological activities of HP536 were only slightly affected by the presence of physiologic concentrations of serum albumin, which seems to be owed to positioning of the albumin-binding sdAb in the middle of the TriTAC molecule.

Two sdAbs were used to engineer HPN536 to achieve high protein stability and to minimize the overall size of the TriTAC. sdAbs were shown to have a higher stability than conventional antibodies and derived fragments that require pairing of heavy and light chain variable domains (50, 51). This may explain the high stability of HPN536 in the circulation of cynomolgus monkeys for up to 7 days, where the TriTAC retained virtually the same biological activity as stored reference material. The inherent stability of sdAbs is retained with alignment of multiple domains on a single polypeptide chain as exhibited by low aggregation propensity. Notably, HPN536 remained monomeric, that is, monovalent, even after incubation for up to 14 days at 40°C (Supplementary Fig. S1). We consider this to be important for HPN536 for reduction of nonspecific T-cell activation and avoidance of off-target T-cell activation in the periphery as can be caused by formation of aggregates, which often is a problem with multivalent anti-CD3 moieties. Finally, the use of a small albumin-binding sdAb for half-life extension in lieu of an Fc-gamma domain allowed reduction of the overall molecular size of TriTACs to a third of an IgG molecule. On theoretical grounds, we hypothesize that the small size and globular shape of HPN536 may improve diffusion into and across tumor tissue (52) for better T-cell engagement and antitumor activity. Although HPN536 binds albumin and possibly soluble MSLN, these interactions are noncovalent. As a result, a small fraction of HPN536 could remain unbound at any given time that can potentially diffuse as an approximately 53-kDa protein and more readily access the tumor microenvironment.

Redirected lysis and T-cell activation by HPN536 was dependent on binding of the TriTAC molecule to MSLN expressed on cancer cells and to CD3ε expressed on T cells. EC_{50} values for MSLN-dependent target cell killing in the range of 0.6–15 pmol/L suggest that formation of a cytolytic synapse between target and T cells required only minute concentrations of HPN536. Nevertheless, target cell lysis and T-cell activation were of highest specificity as they were not observed with cancer cells lacking MSLN expression or with a TriTAC specific for GFP. HPN536 was similarly active across a variety of MSLN-expressing human cancer cell lines from different cancer indications *in vitro* and in xenograft models and against cell lines engineered to express human or cynomolgus monkey MSLN. Of note, HPN536 was designed to bind to mature MSLN as it is retained on the cell surface

Published OnlineFirst December 1, 2020; DOI: 10.1158/1078-0432.CCR-20-3392

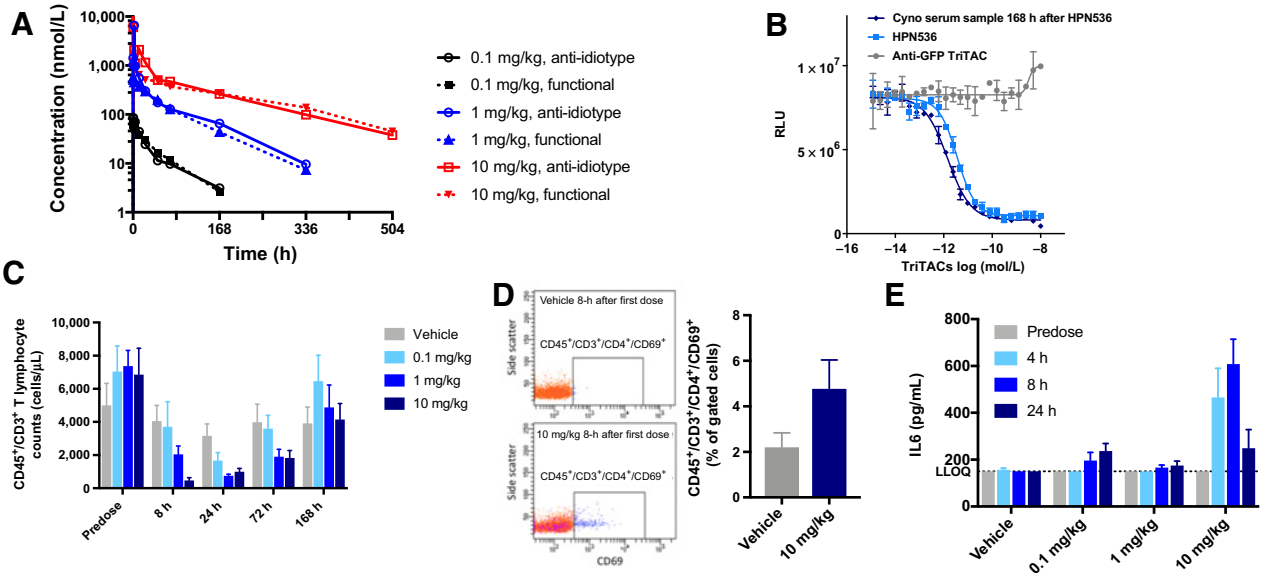

Figure 5.

A single dose of HPN536 was well tolerated with evidence of target engagement in cynomolgus monkeys. **A,** HPN536 serum concentrations after a single intravenous bolus dose to cynomolgus monkeys at doses of 0.1, 1, or 10 mg/kg. For the functional assay, HPN536 was captured with biotinylated CD3ε and subsequently detected with a sulfo-tagged MSLN. For the anti-idiotype assay, HPN536 was captured with an anti-idiotype antibody recognizing the anti-albumin domain and was detected with a sulfo-tagged CD3ε. **B,** TDCC assay comparing the activity of HPN536 in cynomolgus monkey serum pharmacokinetics samples 168 hours after dose, stock HPN536, and control anti-GFP TriTAC. **C,** Transient, dose-dependent, T lymphocyte reduction as demonstrated by flow cytometry analysis of total T cells in blood. **D,** Transient CD69 activation in T lymphocytes by 10 mg/kg HPN536 8 hours after dose. **E,** Serum IL6 cytokine expression following HPN536 administration in cynomolgus monkeys. LLOQ, lower limit of quantitation.

after release of MPF. This way, serum levels of MPF will not impact its activity. The high biological activity, stability, and favorable pharmacokinetics properties of HPN536 support studies testing its clinical activity in patients with MSLN-expressing cancers.

Molecules bridging CD3ε on T cells with a target antigen on cancer cells can organize formation of synaptic structure at the cells' interface that resembles that of a native immunologic synapse as formed between a TCR complex on T cells and peptide-MHC complexes on antigen-presenting cells. Such cytolytic synapses have been described for an EpCAM/CD3-bispecific BiTE molecule (53). They serve as sites for T-cell signal transduction and activation, and as sites for perforin and granzyme release ultimately leading to target cell lysis and caspase 3- and 7-mediated apoptosis (54). The EC_{50} values for redirected lysis by HPN536 were several logs lower than the K_D values measured for HPN536 binding to MSLN and CD3ε, suggesting that very few TriTAC molecules are needed to connect TCRs on T cells with MSLN on tumor cells for cytolytic synapse formation. Cooperative adhesion based on avidity gain and a limited diffusion of HPN536 out of the synaptic structure may be crucial for forming and stabilizing synapses with very few TriTAC molecules.

A close species cross-reactivity of HPN536 between human and cynomolgus monkey MSLN, albumin, and CD3ε provided the basis for a meaningful assessment of pharmacokinetics, pharmacodynamics, and toxicology of HPN536 in the NHP species. While all tested doses led to a transient eclipse of lymphocytes, only the 10 mg/kg dose of HPN536 led to a more robust and transient cytokine release. While

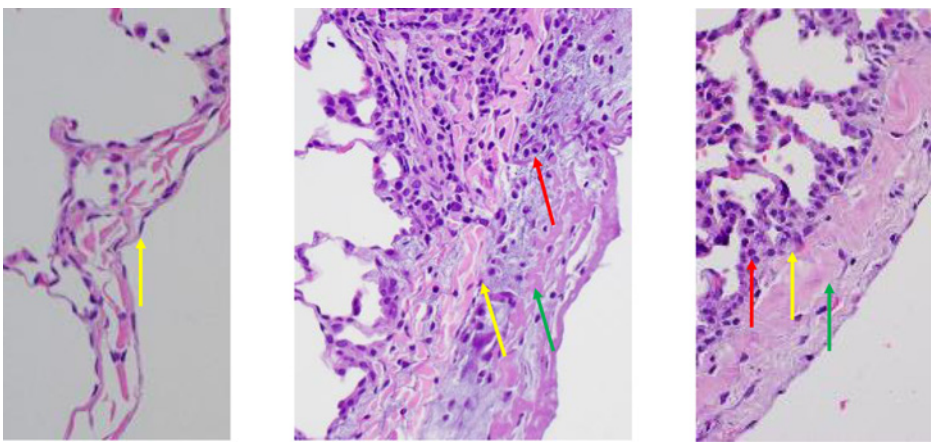

Figure 6.

MSLN-expressing tissues display reversable hyperplasia and inflammation after HPN536 dosing. Vehicle control–treated lung sample (left). Lung sample at necropsy 8 days after HPN536 treatment (left). Lung sample at necropsy 22 days after HPN536 treatment (right). Yellow arrow points to mesothelial border. Red arrow points to immune infiltrates. Green arrow points to extracellular matrix deposition (fibrin and/or collagen).

Published OnlineFirst December 1, 2020; DOI: 10.1158/1078-0432.CCR-20-3392

transient lymphocyte margination does not need T-cell activation, but may be largely governed by a conformational change of cell adhesion molecule LFA-1 on T cells to a high-affinity variant, referred to as inside-out signaling (55), cytokine release and CD69 expression in monkeys were likely to have resulted from synapse formation between T cells and MSLN-expressing normal cells leading to new gene expression. The pharmacodynamic findings with HPN536 in NHPs resemble those of other T-cell–engaging molecules (56, 57). A possible target on normal tissue for HPN536 is the mesothelial cell layer lining cavities, the major tissue expressing MSLN. Reversible hyperplasia and immune infiltrates and matrix deposition observed in the mesothelial linings of treated monkeys support this notion. These dose-dependent histopathologic findings suggest that HPN536 can reach the mesothelial layers and recruit T cells. Simultaneous engagement of MSLN and CD3ε on the mesothelial cells and T cells, respectively, by HPN536 then resulted in redirected lysis of the MSLN-expressing cell layer. As sequalae, other immune cells get attracted, and the mesothelial layer thickens possibly due to an ensuing fibrosis. Despite changes at the microscopic level, HPN536 was remarkably well tolerated at single doses up to 10 mg/kg without gross macroscopic findings or dose-limiting toxicities. Of note, the C_{max} at the 10 mg/kg dose exceeded the highest *in vitro* EC_{50} value for redirected lysis (i.e., 15 pmol/L observed in the HPAFII cells) by a factor of 4×10^5-fold. The pharmacodynamics and toxicology evaluation of HPN536 in the relevant NHP species suggest the potential for a wide therapeutic window.

In conclusion, the current preclinical characterization of HPN536 has provided (i) a scientific rationale to examine the activity of HPN536 in patients suffering from MSLN-expressing cancer, (ii) a further understanding of its potency and mechanism of action, (iii) a basis for calculating the first-in-human clinical dose for a phase I/IIa clinical study based on the recommendation by Saber and colleagues (58), and (iv) a high safety margin in the absence of malignant tissue as shown in a pharmacologic relevant NHP species. An open-label, phase I/IIa study of HPN536 as monotherapy to assess the safety, tolerability, and pharmacokinetics in patients with advanced cancers associated with MSLN expression is currently ongoing (NTC 03872206).

Authors' Disclosures

M.E. Molloy reports a patent for US10543271B2 issued and US20180327508A1 issued. R.J. Austin reports a patent for US10543271B2 issued, US20180327508A1 pending, US20200270362A1 pending, and US9708412B2 issued; reports employment with Harpoon Therapeutics; and has stock and stock options in Harpoon Therapeutics. B.D. Lemon reports a patent for US9920115 issued, US10066016 issued, US10100106 issued, US10543271 issued, US10544221 issued, US10730954 issued, US20180161428A1 pending, US20180162949A1 pending, US20190031749A1 pending, US20190112381A1 pending, US20200270362A1 pending, and US20200289646A1 pending. A. Jones reports other from Harpoon Therapeutics during the conduct of the study. L. Tatalick reports paid nonclinical consultancy for Harpoon. P.A. Baeuerle reports personal fees from Harpoon Therapeutics, Inc. outside the submitted work, as well as a patent 9708412 issued, 20170298149 pending, and 20180162949 pending. C.-L. Law reports full-time employment at Harpoon Therapeutics and owns shares of the company. H. Wesche reports employment with Harpoon and owns shares of Harpoon Therapeutics Inc. No disclosures were reported by the other authors.

Authors' Contributions

M.E. Molloy: Methodology, writing-original draft, writing-review and editing. **R.J. Austin:** Conceptualization, supervision, project administration, writing-review and editing. **B.D. Lemon:** Conceptualization, supervision, project administration, writing-review and editing. **W.H. Aaron:** Formal analysis, investigation, methodology. **V. Ganti:** Formal analysis, methodology. **A. Jones:** Investigation. **S.D. Jones:** Supervision. **K.L. Strobel:** Investigation, methodology. **P. Patnaik:** Investigation. **K. Sexton:** Investigation. **L. Tatalick:** Formal analysis, methodology, writing-review and editing. **T.Z. Yu:** Investigation, methodology. **P.A. Baeuerle:** Conceptualization, writing-review and editing. **C.-L. Law:** Conceptualization, supervision, writing-original draft, project administration. **H. Wesche:** Conceptualization, supervision, funding acquisition, project administration, writing-review and editing.

Acknowledgments

All funding for this work was provided by Harpoon Therapeutics, Inc.

The costs of publication of this article were defrayed in part by the payment of page charges. This article must therefore be hereby marked *advertisement* in accordance with 18 U.S.C. Section 1734 solely to indicate this fact.

Received August 27, 2020; revised October 12, 2020; accepted November 25, 2020; published first December 3, 2020.

References

1. Schuster SJ, Bartlett NL, Assouline S, Yoon S-S, Bosch F, Sehn LH, et al. Mosunetuzumab induces complete remissions in poor prognosis non-Hodgkin lymphoma patients, including those who are resistant to or relapsing after chimeric antigen receptor T-cell (CAR-T) therapies, and is active in treatment through multiple lines. Blood 2019;134:6.
2. Bannerji R, Allan JN, Arnason JE, Brown JR, Advani RH, Barnes JA, et al. Clinical activity of REGN1979, a bispecific human, anti-CD20 x anti-CD3 antibody, in patients with relapsed/refractory (R/R) B-cell non-Hodgkin lymphoma (B-NHL). Blood 2019;134:762.
3. Lugtenburg P, Mous R, Clausen MR, Chamuleau MED, Johnson P, Linton K, et al. First-in-human, phase 1/2 trial to assess the safety and clinical activity of subcutaneous GEN3013 (DuoBody®-CD3×CD20) in B-cell non-Hodgkin lymphomas. Blood 2019;134:758.
4. Patel K, Michot J-M, Chanan-Khan AA, Salles GA, Cartron G, Peyrade F, et al. Preliminary safety and anti-tumor activity of XmAb13676, an anti-CD20 x anti-CD3 bispecific antibody, in patients with relapsed/refractory non-Hodgkin's lymphoma and chronic lymphocytic leukemia. Blood 2019;134:4079.
5. Hutchings M, Iacoboni G, Morschhauser F, Offner F, Sureda A, Salles GA, et al. CD20-Tcb (RG6026), a novel "2:1" format T-cell-engaging bispecific antibody, induces complete remissions in relapsed/refractory B-cell non-Hodgkin's lymphoma: preliminary results from a phase I first in human trial. Blood 2018;132:226.
6. Topp MS, Duell J, Zugmaier G, Attal M, Moreau P, Langer C, et al. Treatment with AMG 420, an anti-B-cell maturation antigen (BCMA) bispecific T-cell engager (BiTE®) antibody construct, induces minimal residual disease (MRD) negative complete responses in relapsed and/or refractory (R/R) multiple myeloma (MM) patients: results of a first-in-human (FIH) phase I dose escalation study. Blood 2018;132:1010.
7. Przepiorka D, Ko C-W, Deisseroth A, Yancey CL, Candau-Chacon R, Chiu H-J, et al. FDA approval: blinatumomab. Clin Cancer Res 2015;21:4035–9.
8. Kebenko M, Goebeler ME, Wolf M, Hasenburg A, Seggewiss-Bernhardt R, Ritter B, et al. A multicenter phase 1 study of solitomab (MT110, AMG 110), a bispecific EpCAM/CD3 T-cell engager (BiTE®) antibody construct, in patients with refractory solid tumors. Oncoimmunology 2018;7:e1450710.
9. Pishvaian M, Morse MA, McDevitt J, Norton JD, Ren S, Robbie GJ, et al. Phase 1 dose escalation study of MEDI-565, a bispecific T-cell engager that targets human carcinoembryonic antigen, in patients with advanced gastrointestinal adenocarcinomas. Clin Colorectal Cancer 2016;15:345–51.
10. Labrijn AF, Janmaat ML, Reichert JM, Parren PWHI. Bispecific antibodies: a mechanistic review of the pipeline. Nat Rev Drug Discov 2019;18:585–608.
11. Austin RJ, Lemon BD, Aaron WH, Barath M, Culp PA, DuBridge RB, et al. TriTACs, a novel class of T cell-engaging protein constructs designed for the

Published OnlineFirst December 1, 2020; DOI: 10.1158/1078-0432.CCR-20-3392

treatment of solid tumors. Mol Cancer Ther 2020 Nov 17 [Epub ahead of print].
12. Chang K, Pastan I. Molecular cloning and expression of a cDNA encoding a protein detected by the ki antibody from an ovarian carcinoma (OVCAR-3) cell line. Int J Cancer 1994;57:90–7.
13. Chang K, Pastan I. Molecular cloning of mesothelin, a differentiation antigen present on mesothelium, mesotheliomas, and ovarian cancers. Proc Natl Acad Sci U S A 1996;93:136–40.
14. Yamaguchi N, Yamamura Y, Konishi E, Ueda K, Kojima T, Hattori K, et al. Characterization, molecular cloning and expression of megakaryocyte potentiating factor. Stem Cells 1996;14:62–74.
15. Chang K, Pastan I, Willingham MC. Isolation and characterization of a monoclonal antibody, K1, reactive with ovarian cancers and normal mesothelium. Int J Cancer 1992;50:373–81.
16. Kaneko O, Gong L, Zhang J, Hansen JK, Hassan R, Lee B, et al. A binding domain on mesothelin for CA125/MUC16. J Biol Chem 2009;284:3739–49.
17. Rump A, Morikawa Y, Tanaka M, Minami S, Umesaki N, Takeuchi M, et al. Binding of ovarian cancer antigen CA125/MUC61 to mesothelin mediates cell adhesion. J Biol Chem 2004;279:9190–8.
18. Bera TK, Pastan I. Mesothelin is not required for normal mouse development or reproduction. Mol Cell Biol 2000;20:2902–6.
19. Hassan R, Kreitman RJ, Pastan I, Willingham MC. Localization of mesothelin in epithelial ovarian cancer. Appl Immunohistochem Mol Morphol 2005;13:243–7.
20. Argani P, Iacobuzio-Donahue C, Rosty C, Goggins M, Wilentz RE, Murugesan SR, et al. Mesothelin is overexpressed in the vast majority of ductal adenocarcinomas of the pancreas: identification of a new pancreatic cancer marker by serial analysis of gene expression (SAGE). Clin Cancer Res 2001;73862–8.
21. Hassan R, Laszik ZG, Lerner M, Raffeld M, Postier R, Brackett D. Mesothelin is overexpressed in pancreaticobiliary adenocarcinomas but not in normal pancreas and chronic pancreatitis. Am J Clin Pathol 2005;124:838–45.
22. Thomas A, Chen Y, Steinberg SM, Luo J, Pack S, Raffeld M, et al. High mesothelin expression in advanced lung adenocarcinoma is associated with KRAS mutations and a poor prognosis. Oncotarget 2015;6:11694–703.
23. Kachala SS, Bograd AJ, Villena-Vargas J, Suzuki K, Servais EL, Kadota K, et al. Mesothelin overexpression is a marker of tumor aggressiveness and is associated with reduced recurrence-free and overall survival in early-stage lung adenocarcinoma. Clin Cancer Res 2014;20:1020–8.
24. Kushitani K, Takeshima Y, Amatya VJ, Furonaka O, Sakatani A, Inai K. Immunohistochemical marker panels for distinguishing between epithelioid mesothelioma and lung adenocarcinoma. Pathol Int 2007;57:190–9.
25. Miettinen M, Sarlomo-Rikala M. Expression of calretinin, thrombomodulin, keratin 5, and mesothelin in lung carcinomas of different types: an immunohistochemical analysis of 596 tumors in comparison with epithelioid mesotheliomas of the pleura. Am J Surg Pathol 2003;27:150–8.
26. Tozbikian G, Brogi E, Kadota K, Catalano J, Akram M, Patil S, et al. Mesothelin expression in triple negative breast carcinomas correlates significantly with basal-like phenotype, distant metastases and decreased survival. PLoS One 2014;9:e114900.
27. Tchou J, Wang LC, Selven B, Zhang H, Conejo-Garcia J, Borghaei H, et al. Mesothelin, a novel immunotherapy target for triple negative breast cancer. Breast Cancer Res Treat 2012;133:799–804.
28. Ordóñez NG. Application of mesothelin immunostaining in tumor diagnosis. Am J Surg Pathol 2003;27:1418–28.
29. Ordóñez NG. Value of mesothelin immunostaining in the diagnosis of mesothelioma. Mod Pathol 2003;16:192–7.
30. Winter JM, Tang LH, Klimstra DS, Brennan MF, Brody JR, Rocha FG, et al. A novel survival-based tissue microarray of pancreatic cancer validates MUC1 and mesothelin as biomarkers. PLoS One 2012;7:e40157.
31. Li M, Bharadwaj U, Zhang R, Zhang S, Mu H, Fisher WE, et al. Mesothelin is a malignant factor and therapeutic vaccine target for pancreatic cancer. Mol Cancer Ther 2008;7:286–96.
32. Morello A, Sadelain M, Adusumilli PS. Mesothelin-targeted CARs: driving T cells to solid tumors. Cancer Discov 2016;6:133–46.
33. Hassan R, Bullock S, Premkumar A, Kreitman RJ, Kindler H, Willingham MC, et al. Phase I study of SS1P, a recombinant anti-mesothelin immunotoxin given as a bolus I.V. infusion to patients with mesothelin-expressing mesothelioma, ovarian, and pancreatic cancers. Clin Cancer Res 2007;13:5144–9.
34. Running Deer J, Allison DS. High-level expression of proteins in mammalian cells using transcription regulatory sequences from the Chinese hamster EF-1alpha gene. Biotechnol Prog 2004;20:880–9.
35. Nazarian AA, Archibeque IL, Nguyen YH, Wang P, Sinclair AM, Powers DA. Characterization of bispecific T-cell Engager (BiTE) antibodies with a high-capacity T-cell dependent cellular cytotoxicity (TDCC) assay. J Biomol Screen 2015;20:519–27.
36. Dixon FJ, Maurer PH, Deichmiller MP. Half-lives of homologous serum albumins in several species. Proc Soc Exp Biol Med 1953;83:287–8.
37. Stevens DK, Eyre RJ, Bull RJ. Adduction of hemoglobin and albumin in vivo by metabolites of trichloroethylene, trichloroacetate, and dichloroacetate in rats and mice. Fundam Appl Toxicol 1992;19:336–42.
38. Lv J, Li P. Mesothelin as a biomarker for targeted therapy. Biomark Res 2019;7:18.
39. Baldo P, Cecco S. Amatuximab and novel agents targeting mesothelin for solid tumors. Onco Targets Ther 2017;10:5337–53.
40. Hassan R, Ebel W, Routhier EL, Patel R, Kline JB, Zhang J, et al. Preclinical evaluation of MORAb-009, a chimeric antibody targeting tumor-associated mesothelin. Cancer Immun 2007;7:20.
41. Brockstedt DG, Giedlin MA, Leong ML, Bahjat KS, Gao Y, Luckett W, et al. Listeria-based cancer vaccines that segregate immunogenicity from toxicity. Proc Natl Acad Sci U S A 2004;101:13832–7.
42. Brahmer J, Johnson ML, Dols MC, RamÌrez S, Coves J, Sukari A, et al. Preliminary immunogenicity, safety, and efficacy of JNJ-64041757 (JNJ-757) in non-small cell lung cancer (NSCLC): results from two phase 1 studies. J Clin Oncol 2019;37:9093.
43. Terwisscha van Scheltinga AG, Ogasawara A, Pacheco G, Vanderbilt AN, Tinianow JN, Gupta N, et al. Preclinical efficacy of an antibody-drug conjugate targeting mesothelin correlates with quantitative 89Zr-ImmunoPET. Mol Cancer Ther 2017;16:134–42.
44. Kreitman RJ, Hassan R, Fitzgerald DJ, Pastan I. Phase I trial of continuous infusion anti-mesothelin recombinant immunotoxin SS1P. Clin Cancer Res 2009;15:5274–9.
45. Hassan R, Sharon E, Thomas A, Zhang J, Ling A, Miettinen M, et al. Phase 1 study of the antimesothelin immunotoxin SS1P in combination with pemetrexed and cisplatin for front-line therapy of pleural mesothelioma and correlation of tumor response with serum mesothelin, megakaryocyte potentiating factor, and cancer antigen 125. Cancer 2014;120:3311–9.
46. Weekes CD, Lamberts LE, Borad MJ, Voortman J, McWilliams RR, Diamond JR, et al. Phase I study of DMOT4039A, an antibody-drug conjugate targeting mesothelin, in patients with unresectable pancreatic or platinum-resistant ovarian cancer. Mol Cancer Ther 2016;15:439–47.
47. Beatty GL, O'Hara MH, Lacey SF, Torigian DA, Nazimuddin F, Chen F, et al. Activity of mesothelin-specific chimeric antigen receptor T cells against pancreatic carcinoma metastases in a phase 1 trial. Gastroenterology 2018;155:29–32.
48. Haas A, Tanyi J, O'Hara M, Gladney W, Lacey S, Torigian D, et al. Phase I study of lentiviral-transduced chimeric antigen receptor-modified T cells recognizing mesothelin in advanced solid cancers. Mol Ther 2019;27:1919–29.
49. Schlereth B, Quadt C, Dreier T, Kufer P, Lorenczewski G, Prang N, et al. T-cell activation and B-cell depletion in chimpanzees treated with a bispecific anti-CD19/anti-CD3 single-chain antibody construct. Cancer Immunol Immunother 2006;55:503–14.
50. Muyldermans S. Nanobodies: natural single-domain antibodies. Annu Rev Biochem 2013;82:775–97.
51. Dumoulin M, Conrath K, Van Meirhaeghe A, Meersman F, Heremans K, Frenken LGJ, et al. Single-domain antibody fragments with high conformational stability. Protein Sci 2002;11:500–15.
52. Thurber GM, Schmidt MM, Wittrup KD. Antibody tumor penetration: transport opposed by systemic and antigen-mediated clearance. Adv Drug Deliv Rev 2008;60:1421–34.
53. Offner S, Hofmeister R, Romaniuk A, Kufer P, Baeuerle PA. Induction of regular cytolytic T cell synapses by bispecific single-chain antibody constructs on MHC class I-negative tumor cells. Mol Immunol 2006;43:763–71.
54. d'Argouges S, Wissing S, Brandl C, Prang N, Lutterbuese R, Kozhich A, et al. Combination of rituximab with blinatumomab (MT103/MEDI-538), a T cell-engaging CD19-/CD3-bispecific antibody, for highly efficient lysis of human B lymphoma cells. Leuk Res 2009;33:465–73.

Published OnlineFirst December 1, 2020; DOI: 10.1158/1078-0432.CCR-20-3392

55. Krummel MF, Bartumeus F, Gérard A. T cell migration, search strategies and mechanisms. Nat Rev Immunol 2016;16:193–201.
56. Chichili GR, Huang L, Li H, Burke S, He L, Tang Q, et al. A CD3xCD123 bispecific DART for redirecting host T cells to myelogenous leukemia: preclinical activity and safety in nonhuman primates. Sci Transl Med 2015;7:289ra82.
57. Ishiguro T, Sano Y, Komatsu SI, Kamata-Sakurai M, Kaneko A, Kinoshita Y, et al. An anti-glypican 3/CD3 bispecific T cell-redirecting antibody for treatment of solid tumors. Sci Transl Med 2017;9:eaal4291.
58. Saber H, Del Valle P, Ricks TK, Leighton JK. An FDA oncology analysis of CD3 bispecific constructs and first-in-human dose selection. Regul Toxicol Pharmacol 2017;90:144–52.

Published OnlineFirst December 1, 2020; DOI: 10.1158/1078-0432.CCR-20-3392

Clinical Cancer Research

Preclinical Characterization of HPN536, a Trispecific, T-Cell–Activating Protein Construct for the Treatment of Mesothelin-Expressing Solid Tumors

Mary Ellen Molloy, Richard J. Austin, Bryan D. Lemon, et al.

Clin Cancer Res Published OnlineFirst December 1, 2020.